Available online at www.sciencedirect.com
ScienceDirect
Computers and Mathematics with Applications 56 (2008) 607–618
An International Journal
computers & mathematics with applications
www.elsevier.com/locate/camwa

A level set evolution strategy in microwave imaging for early breast cancer detection

Natalia Irishina*, Oliver Dorn, Miguel Moscoso

Modelling and Numerical Simulation Group, Universidad Carlos III de Madrid, Avda. de la Universidad 30, 28911 Leganés, Spain

Abstract

In this paper we propose and analyse a novel shape-reconstruction technique for the early detection of breast cancer from microwave data, which is based on a level-set technique. The shape-based approach offers several advantages compared to more traditional pixel-based approaches, as, for example, well-defined boundaries and the incorporation of an intrinsic regularization (in form of a-priori assumptions regarding the general anatomical structures present in the medium) that reduces the dimensionality of the inverse problem and thereby stabilizing the reconstruction. The level set strategy (which is an implicit representation of the shapes) frees us from topological restrictions during this reconstruction process. We present numerical results in 2D which demonstrate the performance of our scheme in various simulated realistic situations.

Keywords: Microwave imaging; Early detection of breast tumours; Shape reconstruction; Level set technique; Tomography

1. Introduction

Microwave tomographic imaging is showing significant promise as a new technique for the early detection of breast cancer. Its physical basis is the high contrast between the dielectric properties of the healthy breast tissue and the malignant tumours at microwave frequencies [1,2]. As a result, tumours have significantly larger microwave scattering cross-sections than the heterogeneities in normal tissue. Several microwave imaging techniques aiming at detecting, localizing and characterizing tumours in the breast are being developed nowadays. Among them, we mention confocal imaging and tomographic systems (see [3–11] and references therein).

Rather than focusing backscattered signal energy as a function of location, microwave tomography solves a nonlinear inverse problem in which a given cost functional is minimized by an iterative scheme [12–15]. We mention that one-step approximate inversions like the Born and Rytov approximations are applied in practice as well, but they are only able to give an indication about the location of an inhomogeneity in the tissue [16,17]. They typically do not yield sufficiently accurate information about the correct size, shape and contrast of a tumour. On the other hand, in classical pixel-based iterative algorithms which go beyond the Born and Rytov approximations it is attempted to achieve successive improvements of an initial guess. This is done by comparing the predicted data corresponding to

* Corresponding author.
E-mail addresses: nirishin@math.uc3m.es (N. Irishina), odorn@math.uc3m.es (O. Dorn), moscoso@math.uc3m.es (M. Moscoso).

0898-1221/$ - see front matter © 2008 Elsevier Ltd. All rights reserved.
doi:10.1016/j.camwa.2008.01.004

the latest estimate of the tumour characteristics with the measured data, and minimizing the resulting least-squares data misfit. In order to stabilize the inversion process, the least-squares data misfit is typically augmented by some additional regularization terms. Unfortunately, the standard Tikhonov–Philips regularization term, usually employed in these strategies, has the effect of 'over-smoothing' the reconstructed images. As a consequence, it is difficult or impossible to accurately estimate key characteristics of the tumour like its shape and its internal dielectric properties. Obtaining these characteristics, on the other hand, could lead to potentially important strategies for breast cancer diagnosis, as described, for example, in [18,19].

In this paper, we propose a novel algorithm for early breast cancer detection which aims at estimating these important characteristics from microwave data. Our results show that our algorithm is able to detect quite small tumours and located them given these data. Moreover, their sizes can be estimated robustly in simulated but realistic situations. The accuracy of the permittivity value estimated by our algorithm when the tumours are very small is mainly limited by the number of data and their signal-to-noisy ratios, but not so much by the range of wavelengths used to illuminate the breast. This is an important observation since so far it is not known whether the classical Rayleigh criterion severely limits the resolution in early breast cancer detection. This increased resolution power, combined with a reliable estimation of the dielectric properties, could lead to a higher specificity between benign and malignant tissues, and may lead to a new strategy to determine whether a normal tissue is in the process of becoming malignant.

We follow in our new algorithm a general approach which has been addressed lately in a variety of applications like diffuse optical tomography, electrical impedance tomography or reservoir characterization (see [20] and references therein), with very promising results. This novel approach formulates the problem as a (generalized) shape reconstruction inverse problem and it is based on a level set technique [21–27]. In the classical version of this approach, it is assumed that the dielectric properties are piecewise constant over the domain with only two possible known values: one for the healthy tissue and another for the tumour. See, for example, the previous work of our group presented in [28]. In the present work, we propose a generalization of this technique which was, in its basic form, introduced in [28]. We follow in our generalization the extended objective of *simultaneously* (i) locating a tumour, (ii) estimating its size, and (iii) characterizing its dielectric properties.

The paper is organized as follows. In Section 2, following this introduction, we describe the mathematical forward model and derive the shape reconstruction technique for early detection of breast tumours which is based on a level set representation of the shapes. Furthermore, we give more technical details of the algorithm. In Section 6 we present and discuss various numerical experiments which demonstrate the performance of our algorithm in, as we believe, representative simulated but realistic 2D situations. Finally, in Section 7 we give some conclusions and mention some open tasks for future research.

2. The forward model

In this paper, our purpose is to develop and evaluate a new reconstruction algorithm for microwave breast tomography. To this end, we consider a heterogeneous 2D medium Ω covered by a layer of skin and illuminated by TM waves (see the top left plot of Fig. 1). In this case, the scalar Helmholtz equation

$$\Delta u + \kappa(\mathbf{x})u = q(\mathbf{x}) \quad \text{in } \Omega, \tag{1}$$

supplemented by the standard *Sommerfeld radiation condition* is a good approximation for describing the nonzero component of the electric field u. In Eq. (1) $\kappa(\mathbf{x}) = \omega^2\mu_0\epsilon_0[\epsilon(\mathbf{x}) + \mathrm{i}\frac{\sigma(\mathbf{x})}{\omega\epsilon_0}]$ is the complex wave number, where ϵ is the relative permittivity and σ is the conductivity. q is the source.

In the level set approach of tumour detection, a so-called 'level set function' is used in order to model the estimated shape of a tumour. The level set technique uses an implicit representation of shapes. The unknown shape S of the tumour is implicitly represented by a so-called 'level set function' $\psi(\mathbf{x})$ as follows. We introduce a sufficiently smooth level set function ψ such that

$$\kappa(\mathbf{x}) = \begin{cases} \kappa_i(\mathbf{x}) \text{ inside } S & \text{where } \psi(\mathbf{x}) \le 0 \\ \kappa_e(\mathbf{x}) \text{ outside } S & \text{where } \psi(\mathbf{x}) > 0. \end{cases} \tag{2}$$

Here, $\kappa_i(\mathbf{x})$ and $\kappa_e(\mathbf{x})$ describe the dielectric properties inside and outside a tumour of shape S, respectively. In our approach, the unknowns of the inversion will be the location and geometry of the tumor, i.e. the level set function ψ

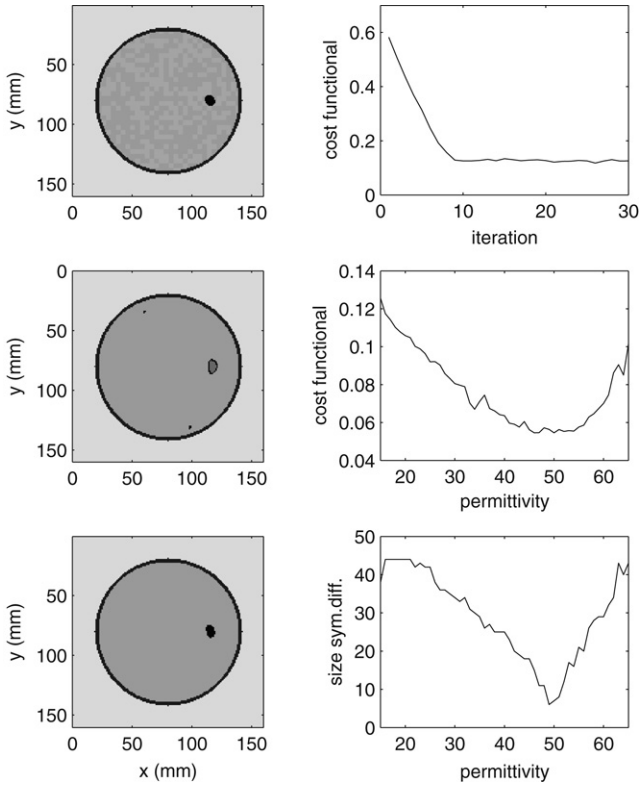

Fig. 1. First numerical experiment: A tumour with the true permittivity value $\epsilon_i = 49$. Tumor size = 63 pixels. Background fluctuations = ±10%. Noise level of data = ±0.5%. Left column from top to bottom: reference permittivity profile (top), reconstructed profile at the end of the first part of the algorithm (centre), and reconstructed profile at the total minimum cost value of the second part of the algorithm (bottom). Right column from top to bottom: evolution of the cost functional (3) during the first part of the algorithm (top), the minimal cost value for each permittivity value during the second part of the algorithm (center), and the size of the symmetrical difference between the true tumour shape and the reconstructed tumour shape for each permittivity value during the second part of the algorithm (bottom). The global minimum of the cost functional during this second part of the algorithm is achieved at the permittivity value $\epsilon_i = 50$.

which models the shape S, as well as the value of the relative dielectric constant ϵ_i inside S. The conductivity value σ_i will be assumed to be known for simplicity. In our future work we will address the more complicated situation where also this value needs to be reconstructed from the data.

Note that there are in general many possible level set functions which can be used for describing the same tumour, and that every continuous function uniquely specifies a tumor by the above definitions. We will indicate the dependence (2) of the parameters κ on the level set function ψ by $\kappa = \kappa[\psi]$. If the level set function is positive everywhere, there is no tumour present in the domain. The boundary of the tumor, δS, consists of all points where $\psi(\mathbf{x}) = 0$. The main advantage of this implicit representation of the unknown shape by a level set function consists of its capability of automatically splitting and merging shapes during the reconstruction, and, in its generalized form as employed here (in the first part of our algorithm), to create and eliminate an arbitrary number of tumours automatically at any step of the algorithm if this is required by the data.

3. The shape reconstruction problem

To solve the shape reconstruction problem for the tumour we will follow a time evolution approach. The goal will be to find an evolution law for the unknown level set function ψ which reduces, and eventually minimizes, the least-squares cost functional

$$\mathcal{J}(\psi) = \frac{1}{2} \|\mathcal{R}(\kappa[\psi])\|^2 . \tag{3}$$

In (3), $\mathcal{R}(\kappa[\psi])$ denotes the mismatch between the true boundary data and those calculated by the forward model using the parameter distribution $\kappa[\psi]$. We consider the general evolution law

$$\frac{\mathrm{d}\psi}{\mathrm{d}t} = f(\mathbf{x}, t) \tag{4}$$

which describes the evolution of the shape S during an artificial time t. Here, the unknown forcing term $f(\mathbf{x}, t)$ needs to be determined from the data in each (artificial) *time step* and $f(\mathbf{x}, t)$ is chosen to point into some descent direction for the cost functional (3).

In order to find such a descent direction, we formally differentiate $\mathcal{J}(\kappa(\psi(t)))$ with respect to the artificial time t and apply the chain rule. We get

$$\frac{\mathrm{d}\mathcal{J}}{\mathrm{d}t} = \frac{\partial \mathcal{J}}{\partial \kappa}\frac{\partial \kappa}{\partial \psi}\frac{\mathrm{d}\psi}{\mathrm{d}t} = \mathtt{Re}\int_{\Omega} \mathcal{R}'(\kappa)^*\mathcal{R}(\kappa)\,(\kappa_e - \kappa_i)\delta(\psi)\, f(\mathbf{x}, t)\mathrm{d}\mathbf{x}, \tag{5}$$

where Re indicates the real part of the corresponding quantity (see [20,28] for a more detailed discussion and a formal derivation of expression (5)). In (5), $\mathcal{R}'(\kappa)^*$ denotes the formal adjoint of the linearized residual operator $\mathcal{R}'(\kappa)$ and the expression $\mathcal{R}'(\kappa)^*\mathcal{R}(\kappa)$ coincides with the pixel-based Frechét derivative of the parameter-to-data mapping of the corresponding parameter reconstruction problem [25]. It will be computed efficiently by using an adjoint scheme. Using Eq. (5), we can select a descent direction for the cost functional by choosing [20]

$$f(\mathbf{x}, t) = -\,\mathtt{Re}\,\left((\kappa_e - \kappa_i)\,\mathcal{R}'(\kappa)^*\mathcal{R}(\kappa)\right) \quad \text{for all } \mathbf{x} \in \Omega. \tag{6}$$

We note that our search direction $f(\mathbf{x}, t)$ has the property that it can be applied even if there is no initial shape available when starting the algorithm (expression (6) is defined and typically nonzero in the whole domain Ω). Therefore, it allows for the creation of objects at any point in the domain, by lowering a positive-valued level set function until its values become negative. This property is useful for avoiding certain types of local minima which often occur in level set formulations that are solely based on the propagation of an already existing shape (where the counterpart to expression (6) is zero or almost zero at large parts of Ω). See again [20] for details.

Numerically discretizing (4) by a straightforward finite difference discretization of the time derivative with time-step $\tau^{(n)} > 0$ in step n, and interpreting $\psi^{(n+1)} = \psi(t^{(n)} + \tau^{(n)})$ and $\psi^{(n)} = \psi(t^{(n)})$ yields the iteration rule

$$\psi^{(n+1)} = \psi^{(n)} + \tau^{(n)}\, f^{(n)}(\mathbf{x}), \qquad \psi^{(0)} = \psi_0. \tag{7}$$

4. Estimation of the dielectrical properties of the tumour

In the previous subsection we assumed that the values corresponding to the dielectrical properties of the tumour and (an average value for) the surrounding tissue were given, even though they might not necessarily match the real values. With these assumptions, our algorithm finds the location and shape of a tumour that minimizes the cost functional (3) for the given dielectric parameters. If these parameters are incorrectly estimated, we expect that the shape will also be slightly incorrect in order to compensate for this error in the model. It is now natural to assume that, if there is any hope at all in reconstructing simultaneously the parameter values and the shape of the tumour from the given data, the final cost value will be the smaller the more we approach the correct values. With this assumption we will get a clearly defined global minimum of the cost functional for the simultaneous estimation of the correct shape and the corresponding correct parameter value. In the following, we want to investigate to what extend this statement is true, and whether it can be used for finding the dielectric properties of the tumour simultaneously with the shape:

To this end, we will start a shape reconstruction with a low relative permittivity equal to $\epsilon_i = 15$. Upon convergence of this initial step, we find the tumour shape that minimizes the cost functional (3) for this parameter value, and we store the minimum value of the cost functional achieved in this search. We then successively increase ϵ_i by one unit $\delta\epsilon$ (in our numerical simulations we choose $\delta\epsilon = 1$) in each step, and we proceed in a similar way by computing the tumour shape that minimizes (3) for these new parameter values storing the corresponding minimum cost values. We stop the search when ϵ_i arrives at some predefined maximal value (which in our case is 65). It is important to remark that in each of these reconstruction steps we start the search of the shape from the final result of the previous permittivitty value. In this way, we have to perform only very few iterations of the shape reconstruction algorithm in

order to achieve convergence. This is so because the optimal shape only changes very little when varying slightly the internal permittivity value.

At the end of this procedure, we obtain a curve corresponding to the achieved minimal values of the cost functional as a function of the relative permittivities ϵ_i. We select the shape and the dielectric properties of the tumour as the solution of the reconstruction problem which corresponds to the global minimum of this curve.

We mention that, in principle, it is also possible to address the simultaneous estimation of the dielectrical tumour parameters together with the shape by incorporating the tumor parameters into the set of unknowns of our evolution problem and looking for descent directions for them in each step of the algorithm. However, our experience is that this strategy does not work well for small tumours due to the existence of many local minima. Therefore, we have chosen to employ the above described alternative technique which is able to find all local and global minima for these additional parameters and the corresponding optimal shapes.

5. Details of the algorithm

In the following, we give some more technical details of our above-described algorithm as employed in our numerical experiments:

We will assume that the breast is composed of three different tissue types of different dielectric properties, namely (a) the surrounding skin, (b) the inhomogeneous healthy breast tissue, and (c) the tumour. Instead of intending to accurately recover the small-scale fluctuations of the dielectric parameters in the healthy breast tissue (which most likely are impossible to recover from the given data), we will model them by predetermined average constant values in the reconstruction process. As we will show in our numerical experiments, this assumption typically yields good results as long as these fluctuations are sufficiently smaller in amplitude than the parameter values of the tumours and can be considered as being more or less randomly distributed in the breast tissue. Our goal will be to detect and characterize very small objects in the breast (tumours in their early stage of development) whose dielectric parameter values are significantly different from those of the fluctuations in the healthy tissue.

To generate simulated data, we model the 'true' breast by assuming that $\kappa_i(\mathbf{x}) = \kappa_i$ is constant and does not depend on position $\mathbf{x}$. $\kappa_e(\mathbf{x})$ is the background distribution consisting of randomly distributed inhomogeneities inside the breast and skin tissue at the boundary of the breast. The same assumptions are made during the reconstruction except that the inhomogeneous breast tissue (without the skin) will be approximated by an average value. Therefore, during the reconstruction $\kappa_e(\mathbf{x})$ will only take two values, one indicating (an averaged value for) background tissue and the other one indicating skin. The thickness and parameter values of the surrounding skin layer are assumed to be known, as well as some average parameter values of the internal background tissue.

As already described, the first stage is devoted to finding the location of the tumour assuming a low parameter value ($\epsilon_i = 15$). In fact, we experimentally find that the location of the tumour is quite robust with respect to the choice of this value and gives about the same location if we choose a different one as long as this value is sufficiently different from the background value, ϵ_e, of the healthy tissue.

We start with a constant positive-valued level set function $\psi^{(0)} > 0$, which means that initially there is no shape present in the domain and no preference is given for any initial location of a tumour. Therefore, the first task of the algorithm will be to 'create' one or more objects at positions where the probability of a tumour is high. We refer here the reader to the discussion given in [20] on the creation of objects in a level set-based shape reconstruction scheme. Then, we apply (7) with $f^{(1)}$ given by (6). As step-size criterion for the choice of $\tau^{(1)}$ in (7) we look for the smallest choice of $\tau^{(1)}$ which changes approximately (and preferably not more than) 5 pixel values in the domain. (Notice that this step-size criterion does not require to run additional forward or adjoint problems (1) and is therefore without additional computational cost.) This means that after applying the update (7) in the first step of the algorithm, a small shape (about 5 pixels in size) will be created at a location indicated by the sensitivity structure of the data. Then, we continue deforming this shape by calculating iteratively new forcing terms $f^{(n)}$ and the corresponding new corrections of the level set function updating the latest best guess. Each of these new steps uses the data of 5 frequencies (between 0.5 and 2 GHz) one after the other, which yields a so-called 'sweep' of our algorithm. In each update we choose a step-size such that about 5 pixel values change at this update. (Hitting exactly the target value of 5 pixels is sometimes difficult, in which cases we allow for fewer or more pixels to change in these updates). During this first part of the inversion, 30 sweeps are applied in order to optimize the initial shape corresponding to the parameter value $\epsilon_i = 15$. At the end of this initial loop, we have found an optimized shape and a corresponding value of the least squares cost

functional which are the final result of this initial reconstruction procedure. Thereafter, we start the second part of our algorithm whose aim is to optimize simultaneously the parameter value inside the tumour and its shape.

During this second stage of the algorithm, we continue in an efficient way by probing the corresponding minimal cost values achieved by the next higher permittivity values. Accordingly, we increase the value of ϵ_i by a fixed small step-size $\delta\epsilon$, and repeat the above search for the shape starting from the reconstructed shape corresponding to $\epsilon_i = 15$ but now assuming the value $\epsilon_i = 15 + \delta\epsilon$. Then we continue with the permittivity value $\epsilon_i = 15 + 2\delta\epsilon$ using as starting guess the reconstructed shape for $\epsilon_i = 15 + \delta\epsilon$. During this second stage we restrict (6) to a narrowband in a small neighbourhood of the tumour shape at each iteration. Mathematically, this 'narrowband strategy' amounts to incorporating the Dirac delta function $\delta(\psi)$ of (5) (which is concentrated at the boundary of the current shape) in the choice of the descent direction (6). We approximate this additional factor of (6) by a function which is one in a small neighbourhood of the shape boundary and zero elsewhere. Doing so, we suppress in this second part the ability of our level set updates to create new shapes far away from already existing ones. Since we already have found the location(s) of the possible tumour(s) at this stage of the algorithm, no new shapes are desired in this second part. Instead, we can concentrate on refining the details of the already discovered shape(s). Moreover, in order to achieve more refined details in this second part, we restrict the line search criterion to a change of at most 2 pixels per update. (Again, in very few updates it might happen that it is difficult to achieve this step-size, in which cases a different number of pixels is allowed to change). We perform from 5 to 10 iterations for the set of 5 frequencies per permittivity value, and we store: (i) the minimum value of the cost functional (3), and (ii) the size of the 'symmetrical difference' between the real and the reconstructed tumours (i.e. the added number of pixels which either belong to the correct tumour but not to the reconstructed one, or belong to the reconstructed tumour but not to the correct one). Once we have found these values for each probing permittivity, we search for the global minimum of the cost functional and interpret the corresponding permittivity value of the tumour and its corresponding shape as the reconstructed estimates of tumour characteristics. We emphasize that the size of the symmetrical difference is monitored here only in order to investigate and validate the performance of our algorithm, but that it is not used in the reconstruction task itself (because it would require the knowledge of the correct tumour shape).

6. Numerical experiments

In the numerical experiments presented here we investigate a 2D tomographic configuration as shown in the top left image of Fig. 1. In our experimental setup, a 12.0 cm-diameter breast, covered by a 3 mm-thick skin layer, is immersed in a matching fluid environment. 40 'transducers' are equidistantly distributed around the breast. The transducers illuminate it, one after the other, with microwaves of different frequencies. We use here 0.5, 0.8, 1.0, 1.5 and 2.0 GHz. The average relative permittivity and conductivity values for the breast tissue (background medium) are assumed to be $\epsilon_e = 9$ and $\sigma_e = 0.4$ S/m, respectively. To simulate the heterogeneity of the normal breast tissue, as measured by Chaudhary et al. [1] and Joines et al. [29], we add random variations of $\pm 10\%$, distributed over $4 \times 4\text{mm}^2$ squares, around these values. The skin layer has a permittivity value of $\epsilon_{\text{skin}} = 34$ and a conductivity value of $\sigma_{\text{skin}} = 1$ S/m. The surrounding 'matching' fluid medium is chosen to be slightly lossy with values $\epsilon_{\text{liquid}} = 2.5$ and $\sigma_{\text{liquid}} = 0.04$ S/m.

It is one of our goals in this paper to investigate if our algorithm is able to specify the dielectric properties of a detected tumour together with its location and approximate size. For this purpose, we will apply our algorithm to two different types of tumours, the first one having a constant permittivity value of $\epsilon_i = 36$ and the second one having the value $\epsilon_i = 49$. Both tumors have a conductivity value of $\sigma_i = 4$ S/m. We consider tumours with different sizes and positions in our numerical experiments. The combination of all reliably estimated characteristics for a given tumour (dielectric properties, size, shape, etc.) could help the physician in the task of characterizing a detected tumour as 'benign' or 'malignant'.

We solve (1) with a second order finite differences scheme and a perfectly matched layer (PML) for numerically terminating the computational domain. We use a mesh of 160×160 pixels. Each pixel is a square of 1×1 mm^2. The numerically simulated 'true' data (corresponding to the assumed 'true' breast) is perturbed by $\pm 0.5\%$ white Gaussian noise. In the following we show several results for breast imaging that illustrate the performance and robustness of our level set-based algorithm.

Fig. 1 shows the results for a tumour that is located 2.0 cm beneath the surface. In this numerical setup, the tumour has a size of 63 pixels and its 'true' permittivity value is $\epsilon_i = 49$. The remaining values are as described previously.

The top left image of this figure shows the 'true' permittivity profile. During the first part, the algorithm tries to detect whether there is a tumour, and if so, to find its approximate location. For this, a low permittivity value $\epsilon_i = 15$ of the tumour is assumed (being actually quite far from the 'true' one $\epsilon_i = 49$). The centre image of the left column of the figure shows the final reconstruction after 30 sweeps or iterations of this first part of the algorithm. Each sweep uses each of the five frequencies exactly once. The top right image of the figure displays the evolution of the cost functional (3) during these 30 iterations. It is apparent that the cost functional (as well as the corresponding reconstructed shape) stabilizes after about 10 iterations at a relatively low cost value. A comparison of the reconstructed tumour with the correct one (displayed in the top left image of the figure) demonstrates that (i) the tumor has been detected reliably (ii) its location has been estimated correctly and (iii) its size has been approximated quite well taking into account that the permittivity value assumed for the reconstructed tumour is incorrect and far away from the true one. Certainly, the reconstructed size can be improved, as will be done during the second part of the algorithm when searching also for the correct parameter value.

The second part of the algorithm starts with the reconstruction of the first part as an initial guess. It minimizes the cost functional in only few iterations for a set of equidistant permittivity values between $\epsilon_i = 15$ and $\epsilon_i = 65$. For demonstration purposes we used here 10 iterations for each permittivity value, even though fewer would suffice. This minimized cost functional is displayed in the center image of the right column of Fig. 1 as a function of the permittivity value. Once this second part has been completed, we look for the global minimum of this curve and we take the corresponding permittivity value and its shape as the estimates of the tumour characteristics. We plot in the bottom left image of Fig. 1 our final estimated shape.

In order to monitor the quality of our reconstruction, and taking advantage of the fact that in our 'simulated' setup we actually 'know' the true tumour, we plot in the bottom right image of Fig. 1 the size of the symmetrical difference (in number of pixels) between the reconstructed tumour and the true tumour shapes. We observe that both curves (displayed in the centre and the bottom of the right column) show a clear minimum around the 'true' permittivity value $\epsilon_i = 49$. We conclude from this observation that our algorithm has been able not only to estimate the true permittivity value sufficiently well, but also to provide us with a good estimate of the corresponding size of its shape: only very few (of the order of five) pixels are estimated incorrectly at this minimum value of the cost.

The second numerical experiment, whose results are displayed in Fig. 2, is designed in order to investigate the limitations of the second part of our algorithm in the task of simultaneously estimating the parameter values of a tumour which has been detected and correctly located during the first part of the algorithm. A small tumour of only 23 pixels and a permittivity value of $\epsilon_i = 49$ is located at 3.0 cm beneath the surface. Here the question arises which level of noise (in particular background fluctuations) can be tolerated in cases that the size of the tumour is very small and the tumour is located quite deep in the breast. We display in the four images of the Fig. 2, subtitled as 'experiment 2 (a)', the reconstruction of our algorithm assuming that the background fluctuations are at the level of $\pm 5\%$ (as usual we also have added here $\pm 0.5\%$ of additive noise in the data). In the top left and bottom left images we plot the 'true' and the reconstructed permittivity profiles, respectively. In the top right image we plot the minimal cost value for each permittivity, and in the bottom right image we plot the size of the symmetrical difference between true and reconstructed tumours. In Fig. 3, subtitled as 'experiment 2 (b)', we show the reconstruction for the same situation but with stronger background fluctuation at the level of $\pm 10\%$. The arrangement of images in 'experiment 2 (b)' is the same as in 'experiment 2 (a)'. We observe that, for such a small and deeply located tumour, a reliable estimate of the true permittivity value can still be achieved by the algorithm for the case of $\pm 5\%$ background fluctuations, but that this is no longer possible if the background fluctuations reach the level of $\pm 10\%$. In the latter case, no clear minimum of the cost functional with respect to the permittivity value can be found during the second part of the algorithm. Nevertheless, we want to emphasize that in both experiments the presence of the tumour is still clearly detected by our algorithm, along with a good estimate of its size.

A more systematic investigation of the limitations of the algorithm for the purpose of the simultaneous reconstruction of its size and permittivity value is displayed in Fig. 4. This study can also provide indications of the limitations of more general microwave imaging systems for this purpose. The general setup of this experiment is the same as that used in Fig. 1. However, three limiting factors of the algorithm are now modified: (i) the level of unknown background fluctuations of the parameters, (ii) the level of noise added to the data, and (iii) the conductivity value of the skin. Note that a high conductivity value of the skin has a 'shielding-effect' since the probing microwaves cannot easily penetrate into the breast.

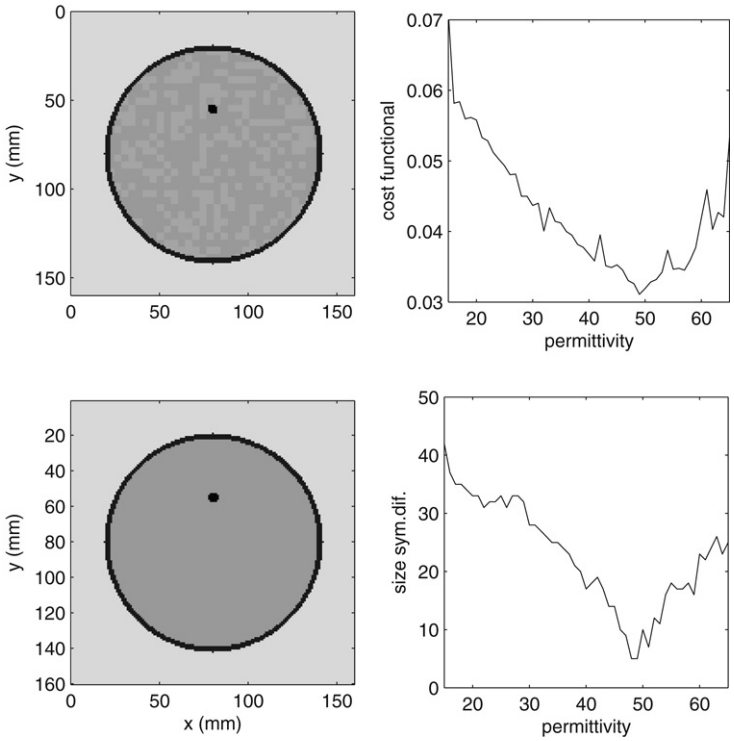

Fig. 2. Experiment 2 (a): A very small tumour. Tumour size = 23 pixels. True permittivity value $\epsilon_i = 49$. The tumour is located deep in the breast. The objective of this experiment is to show the limitations of the algorithm for the simultaneous determination of size and parameter values of deeply located small tumours in relation to the level of the background fluctuations in the breast. Shown are reconstructions of the tumour assuming ±5 per cent of background tissue fluctuations. We display a block of four images, of each of which the top left shows the true permittivity profile, the bottom left shows the final reconstruction of part 2 of the algorithm, the top right shows the minimum value of the cost functional for each permittivity value during the second part of the algorithm, and the bottom right image shows the size of the corresponding symmetrical difference between the true shape of the tumour and the reconstructed shape for each permittivity value.

As one part of this comparison we assume that the correct ('true') shape of the tumour has been found and only the permittivity value needs to be reconstructed. In other words, we assume the prior knowledge of the location and exact shape of the tumour. In the upper image of Fig. 4 we display the least squares mismatch (3) between the 'true' (noisy) data and those data which have been calculated assuming probing permittivity values between $\epsilon_i = 15$ and $\epsilon_i = 65$. It is clear that a very flat curve of the least squares cost (3) with respect to the permittivity value will make it very difficult for the algorithm to estimate the correct permittivity value by a least squares search. In this case, the least squares cost does not depend significantly on the permittivity value. The exact parameter values corresponding to each of the curves from (1) to (5) are explained in detail in the caption of the figure. Interpreting these curves, we expect that the situations with a moderate level of noise in the data, represented by curves (1), (2) and (4), will allow us to reliably determine the permittivity value in addition to size and location of the tumor. These curves show sufficient variation of the least squares cost (3) with respect to the permittivity value (a 'gradient' or 'slope' being sufficiently different from zero). On the other hand, the situations (3) and (5), where the level of noise in the data has been increased, are expected to make it hard to recover these characteristics simultaneously with the shape. In these cases, the corresponding curves are almost flat (their slope or gradient almost being zero) in a large neighbourhood of the correct permittivity value. From this figure, we conclude that the level of additive noise in the data is one of the more limiting factors in the simultaneous reconstruction of shape and permittivity value of the tumour, whereas the background fluctuations and the conductivity value of the skin are less restrictive.

As the other part of this comparison, we show in the bottom image of Fig. 4 the results when the correct shape of the tumour is assumed to be unknown. In other words, the corresponding curves achieved during this second part of the comparison take into account the simultaneous reconstruction of both the shape and the permittivity value of the tumour in order to minimize (3). These curves are those which correspond to the centre right images of Fig. 1

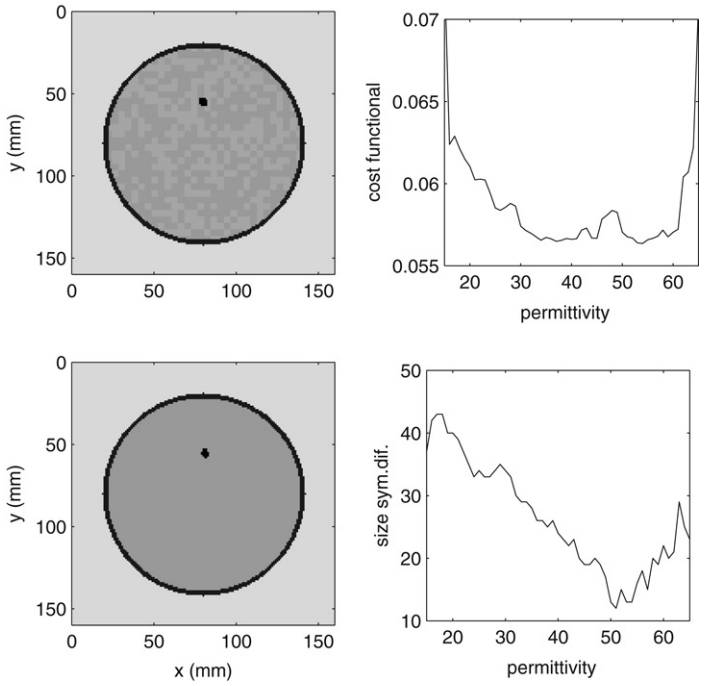

Fig. 3. Experiment 2 (b): Same as in Fig. 2 but with ±10 of percentage background tissue fluctuations.

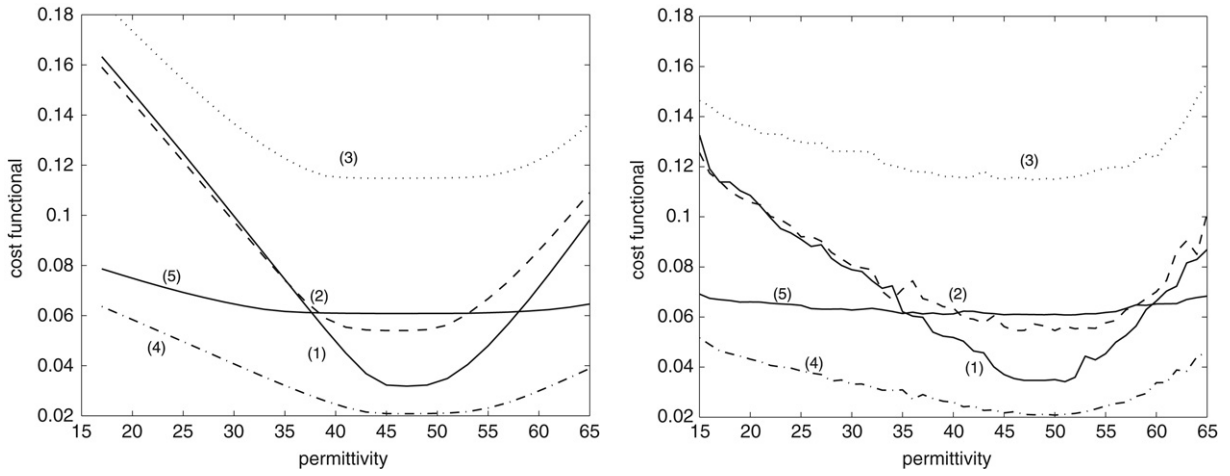

Experiment 3(a): Cost assuming true tumour shape.

Experiment 3(b): Cost for reconstructed tumour shape.

Fig. 4. The graphs in the top image of the figure (experiment 3 (a)) display the values of the cost functional for each permittivity value between $\epsilon_i = 15$ and $\epsilon_i = 65$ assuming that the correct shape of the true tumor is known. The graphs in the bottom image show the corresponding calculated cost values assuming instead the shapes which have been reconstructed by the algorithm for each permittivity value. The individual graphs of both images correspond to the following situations. Graph (1) (solid): ±5% background fluctuations, ±0.5% noise in the data, conductivity of surrounding skin $\sigma_s = 1$ S/m; graph (2) (dashed): same as in graph (1) but with ±10% background fluctuations; graph (3) (dotted): same as in graph (1) but with ±2.5% noise in the data; graph (4) (dash-dotted): same as in graph (1) but with $\sigma_s = 4$ S/m; graph (5) (solid): ±10% background fluctuations, ±1.5% noise in the data and $\sigma_s = 4$ S/m (the most 'difficult' case considered here). The 'flatter' a given curve is, the more difficult it will be for the algorithm to find the correct global minimum of the combined cost functional in the simultaneous search for shape and permittivity value.

(the second part of our reconstruction algorithm) when assuming the modified values as used here. Comparing these curves with those of the upper image, we see that our algorithm reproduces their general tendency without knowing the correct shape. We observe, though, that the slopes of the curves obtained in the lower image are in general smaller

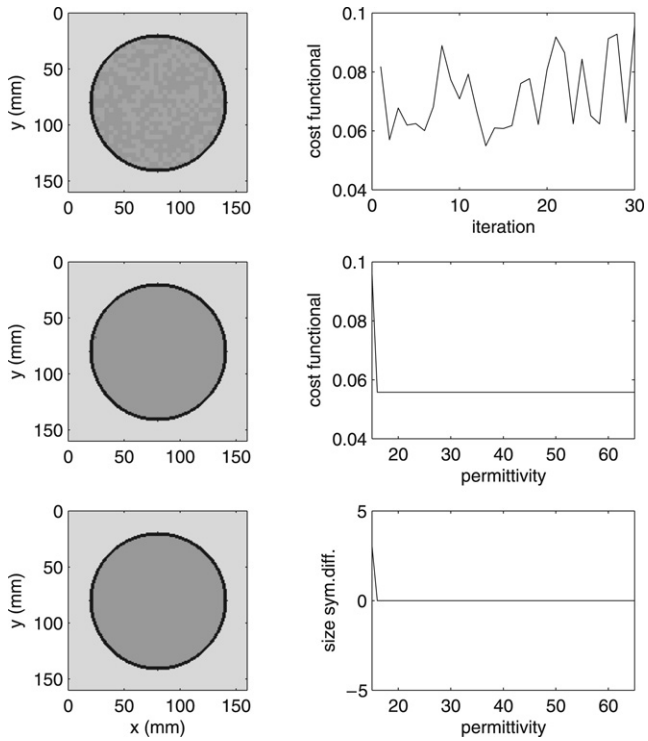

Fig. 5. The same situation and arrangement of images as described in Fig. 1, but now without a tumour present in the 'true' breast. The objective of this experiment is to verify whether the algorithm can reliably distinguish between the situation with a tumour present in the 'true' breast and that one without a tumour present assuming random background fluctuations of about $\pm 10\%$ in the parameters of the breast tissue and $\pm 0.5\%$ of noise in the data.

(their gradients being closer to zero) than those of the upper image, and that the achieved minimized cost values are also slightly smaller. This behaviour is due to the fact that an incorrectly assumed permittivity value during the reconstruction can partly be compensated by the algorithm by producing a slightly modified shape. Nevertheless, this 'compensation effect' is not significant and does not change the location of the total minimum of these curves. Therefore, the simultaneous detection of size and permittivity value is indeed possible, as long as the curves shown in the upper image (which assume a perfectly reconstructed shape) have a sufficiently pronounced total minimum. Notice also that the cost value achieved by our algorithm when probing with the 'correct' permittivity value of $\epsilon_i = 49$ is almost identical to the one shown in the upper image, which indicates that our algorithm has been able to provide a very good approximation to the true shape of the tumour.

Finally, Fig. 5 displays the results of our algorithm in a situation where no tumour is actually present in the breast. The arrangement of images in this figure is the same as in Fig. 1. The natural question that arises here is whether the typical but unknown background fluctuations, and the noise in the data, might give rise to 'ghosts' in the reconstructions which could be interpreted as a tumour (a 'false positive'). Recall that during the first part of our algorithm we artificially enforce the creation of a tumour in the first step. Since the initial guess does not contain a tumour, there is no other way to start the search than to create a tumour. We observe, however, that during the first part of the algorithm this created tumour does not grow, but instead is repeatedly removed. It might reappear at some later iteration, maybe at some other location, but also then it is removed by following iterations. We observe that none of these 'ghost objects' during the iterations of the first part behaves stably, such that this first part already indicates that there is in fact no tumour present. The evolution of the cost functional (3) during this part of the algorithm shows highly erratic oscillations around the noise level 0.05 (see the top right image of Fig. 5), not showing any clear tendency of reduction for a given reconstruction. The final result of this first part is, in this particular case, a small 'ghost' whose size consists of very few pixels (less than 5). As it can be seen, the first iterations of the second part of the algorithm removes this 'ghost tumour' immediately, such that it is lost permanently. The now added 'narrowband' does not allow for the creation of a new tumour: a shape which has been removed completely during the second part of

the algorithm cannot be recovered. The final cost value remains constant at the value which represents the background fluctuations and the additional noise in the data. Moreover, the 'final shape' is empty, indicating correctly that there is no tumour present in the domain. Notice that it is already apparent at the end of the first part of the algorithm that there is no tumour (since the cost is not clearly reduced), such that it is not really necessary to perform the second part if there is no tumour present.

7. Conclusions

We have presented a novel shape-based algorithm for the early detection and characterization of breast tumours from microwave data. A level set technique has been employed in order to free the iterative algorithm from topological restrictions. The presented algorithm consists of two parts. The goal of the first part is to detect a tumour and to give a first estimate of its location and size. The second part starts with the result of the first part and aims at refining the information of location and size of the tumour while at the same time estimating its correct permittivity value. We have shown that the task of detecting and locating a hidden tumor by our algorithm is very stable and reliable. If there is no tumour present in the breast, the algorithm may create ghost objects during its first part due to the chosen line search criterion. However, these ghost objects are small and unstable and change location during the iteration, and, more importantly, the behaviour of the cost functional during the first part shows clearly that these objects cannot be interpreted as true tumours. Moreover, the 'ghost objects' disappear automatically during the first few steps of the second part of the algorithm due to the chosen narrowband strategy. Once a 'true' tumour has been detected and localized, the second part of the algorithm is able to reliably estimate its correct permittivity value simultaneously with its size and location. Only for very small tumours which are hidden deep in the breast, and in the presence of strong data noise, this characterization task of the tumour fails (we emphasize again that the detection and location task of the algorithm is not affected by these severe conditions). We have shown that in this case the least squares cost functional is nearly flat in a large neighbourhood of the correct values (its 'slope' or 'gradient' is almost zero) and does not show a clear global minimum at the correct permittivity value. Different algorithms, aiming at simultaneously minimizing the least squares cost with respect to both the permittivity value and tumour shape by a strict gradient scheme, might trigger the stopping criterion at a premature and wrong permittivity value in these situations due to local minima. The flat cost functionals explain why our criterion based on minimizing this least squares cost functional cannot be applied in these situations.

On the other hand, we have shown that the possible alternative limitations caused by a high conductivity value of the skin or by the internal parameter fluctuations of healthy breast tissue (of a level typically found in breast tissue) are less severe in our numerical experiments and can be dealt with by the algorithm as long as the additive data noise is kept below a certain threshold (a level of $\pm 0.5\%$ is well acceptable). In our future research we plan to generalize our algorithm by incorporating also the conductivity value of the tumour in the reconstruction task, and by extending the algorithm to a more realistic 3D situation with preferably a more detailed reconstruction of more shape details from a richer data set.

Acknowledgments

The authors thank Dr. Magda El-Shenawee for very interesting discussions and useful comments. This work was financed by the Spanish Ministry of Education and Science, Grant no. FIS2004-03767 and FIS2007-62673, and by the Autonomous Region of Madrid (Grant. no. S-0505/ENE/0229, COMLIMAMS).

References

[1] S.S. Chaudhary, R.K. Mishra, A. Swarup, J.M. Thomas, Dielectric properties of normal and malignant human breast tissues at radiowave and microwave frequencies, Ind. J. Biochem. Biophys. 21 (1984) 76–79.

[2] C. Gabriel, S. Gabriel, R.W. Lau, E. Corthout, The dielectric properties of biological tissues: Part I, II, and III, Phy. Med. Biol. 41 (1996) 2231–2249.

[3] C.E. Fear, S.C. Hagness, P.M. Meaney, M. Okoniewski, M.A. Stuchly, Breast tumor detection, IEEE Microwave Mag. (March) (2002) 48–56.

[4] S.C. Hagness, A. Taflove, J.E. Bridges, Two-dimensional FDTD analysis of a pulsed microwaved confocal system for breast cancer detection: fixed-focus and antenna-array sensors, IEEE Trans. Antennas Propagat. 45 (1998) 1470–1479.

[5] S.C. Hagness, A. Taflove, J.E. Bridges, Three-dimensional FDTD analysis of a pulsed microwaved confocal system for breast cancer detection: Design of an antenna-array element, IEEE Trans. Antennas Propagat. 47 (1999) 783–791.

[6] E.C. Fear, M.A. Stuchly, Microwave system of breast cancer, IEEE Microwave Guided Wave Lett. 9 (1999) 470–472.
[7] X. Li, S.C. Hagness, A confocal microwave imaging algorithm for breast cancer detection, IEEE Microwave Wireless Components Lett. 11 (2001) 130–132.
[8] M.A. Hernández-López, M. Quintillán-González, S. González García, A. Rubio Bretones, R. Gómez Martín, A rotating array of antennas for confocal microwave breast imaging, Microwave Optical Tech. Lett. 39 (2003) 307–311.
[9] E.J. Bond, X. Li, S.C. Hagness, B.D. Van Veen, Microwave imaging via space-time beamforming for early detection of breast cancer, IEEE Trans. Antennas Propagat. 51 (2003) 1690–1705.
[10] X. Li, S.C. Hagness, B.D. Van Veen, D. van der Weide, Experimental investigation of microwave imaging via space-time beamforming for breast cancer detection, IEEE MTT-S Int. Microwave Symp. Dig. (2003) 379–382.
[11] L. Borcea, G. Papanicolaou, C. Tsogka, Theory and applications of time reversal and interferometric imaging, Inverse Problems 19 (2003) 5139–5164.
[12] P.M. Meaney, M.W. Fanning, D. Li, S.P. Poplack, K.D. Paulsen, A clinical prototype for active microwave imaging of the breast, IEEE Trans. Microwave Theory Tech. 48 (2000) 1841–1853.
[13] P.M. Meaney, K.D. Paulsen, M.W. Fanning, Microwave imaging for breast cancer detection: Preliminary experience, Proc. SPIE-Int. Soc. Opt. Eng. 3977 (2000) 308–319.
[14] A.E. Souvorov, A.E. Bulyshev, S.Y. Semenov, R.H. Sveson, G.P. Tatsis, Two-dimensional computer analysis of a microwave flat antenna array for breast cancer tomography, IEEE Trans. Microwave Theory Tech. 48 (2000) 1413–1415.
[15] A.E. Bulyshev, S.Y. Semenov, A.E. Souvorov, R.H. Sveson, A.G. Nazarov, Y.E. Sizov, G.P. Tatsis, Computational modeling of three-dimensional microwave tomography of breast cancer, IEEE. Trans. Biomed. Eng. 48 (2001) 1053–1056.
[16] L. Jofre, M.S. Hawley, A. Broquetas, E. de los Reyes, M. Fernando, A.R. Elias-Fuste, Medical imaging with a microwave tomographic scanner, IEEE Trans. Biomed. Eng. 37 (1990) 303–312.
[17] A. Broquetas, J. Romeu, J.M. Ruis, A.R. Elias-Fuste, A. Cardama, L. Jofre, Cylindrical geometry: A further step in active microwave tomography, IEEE Trans. Microwave Theory Tech. 39 (1991) 836–844.
[18] M. El-Shenawee, E.L. Miller, Spherical harmonics microwave algorithm for shape and location reconstruction of breast cancer tumor, IEEE Trans. Med. Imag. 25 (2006) 1258–1271.
[19] B. Alberts, D. Bray, J. Lewis, M. Raff, K. Roberts, J.D. Watson, Molecular Biology of the Cell, 2nd ed., Garland, New York, 1989, Chapter 10.
[20] O. Dorn, D. Lesselier, Level set methods for inverse scattering, Inverse Problems 22 (2006) R67–R131.
[21] O. Dorn, E. Miller, C. Rappaport, A shape reconstruction method for electromagnetic tomography using adjoint fields and level sets, Inverse Problems 16 (2000) 1119–1156.
[22] A. Litman, Reconstruction by level sets of n-ary scattering obstacles, Inverse Problems 21 (2005) 1–22.
[23] C. Ramananjaona, M. Lambert, D. Lesselier, Shape inversion from TM and TE real data by controlled evolution of level sets, Inverse Problems 17 (2001) 1585–1595.
[24] F. Santosa, A level set approach for inverse problems involving obstacles, ESAIM Control Optim. Calculus Variations 1 (1996) 17–33.
[25] M. Schweiger, S.R. Arridge, O. Dorn, A. Zacharopoulos, V. Kolehmainen, Reconstructing absorption and diffusion shape profiles in optical tomography using a level set technique, Optics Lett. 31 (4) (2006) 471–473.
[26] R. Villegas, O. Dorn, M. Moscoso, M. Kindelan, F. Mustieles, Simultaneous characterization of geological shapes and permeability distributions in reservoirs using the level set method, Society of Petroleum Engineers SPE paper 100291, SPE Europec/EAGE Annual Conference and Exhibition, Vienna, Austria, June 12–15, 2006 (Proc. paper C015, pp. 1–12).
[27] X.C. Tai, T.F. Chan T F, A survey on multiple level set methods with applications for identifying piecewise constant functions, Internat. J. Numer. Anal. Modeling 1 (1) (2004) 25–47.
[28] N. Irishina, M. Moscoso, O. Dorn, Detection of small tumors in microwave medical imaging using level sets and MUSIC, Proc. PIERS, Cambridge (2006) 43–47.
[29] W.T. Joines, Y. Zhang, C. Li, R.L. Jirtle, The measured electrical properties of normal and malignant human tissues from 50 to 900 MHz, Med. Phys. 21 (1994) 547–550.